JACS
JOURNAL OF THE AMERICAN CHEMICAL SOCIETY

Article
pubs.acs.org/JACS

Differentiating between Trivalent Lanthanides and Actinides

Matthew J. Polinski,[†] Daniel J. Grant,[‡] Shuao Wang,[†] Evgeny V. Alekseev,[§,∥] Justin N. Cross,[†] Eric M. Villa,[†] Wulf Depmeier,[⊥] Laura Gagliardi,[‡] and Thomas E. Albrecht-Schmitt*,[†]

[†]Department of Chemistry and Biochemistry and Department of Civil Engineering and Geological Sciences, University of Notre Dame, 156 Fitzpatrick Hall, Notre Dame, Indiana 46556, United States

[‡]Department of Chemistry and Supercomputing Institute, University of Minnesota, 207 Pleasant Street SE, Minneapolis, Minnesota 55455, United States

[§]Forschungszentrum Jülich GmbH, Institute for Energy and Climate Research (IEK-6), 52428 Jülich, Germany

[∥]Institut für Kristallographie, RWTH Aachen University, D-52056 Aachen, Germany

[⊥]Institut für Geowissenschaften, Universität zu Kiel, 24118 Kiel, Germany

Supporting Information

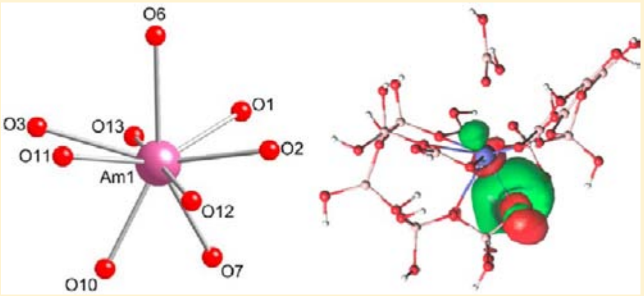

ABSTRACT: The reactions of $LnCl_3$ with molten boric acid result in the formation of $Ln[B_4O_6(OH)_2Cl]$ (Ln = La−Nd), $Ln_4[B_{18}O_{25}(OH)_{13}Cl_3]$ (Ln = Sm, Eu), or $Ln[B_6O_9(OH)_3]$ (Ln = Y, Eu−Lu). The reactions of $AnCl_3$ (An = Pu, Am, Cm) with molten boric acid under the same conditions yield $Pu[B_4O_6(OH)_2Cl]$ and $Pu_2[B_{13}O_{19}(OH)_5Cl_2(H_2O)_3]$, $Am[B_9O_{13}(OH)_4]\cdot H_2O$, or $Cm_2[B_{14}O_{20}(OH)_7(H_2O)_2Cl]$. These compounds possess three-dimensional network structures where rare earth borate layers are joined together by BO_3 and/or BO_4 groups. There is a shift from 10-coordinate Ln^{3+} and An^{3+} cations with capped triangular cupola geometries for the early members of both series to 9-coordinate hula-hoop geometries for the later elements. Cm^{3+} is anomalous in that it contains both 9- and 10-coordinate metal ions. Despite these materials being synthesized under identical conditions, the two series do not parallel one another. Electronic structure calculations with multireference, CASSCF, and density functional theory (DFT) methods reveal the An 5f orbitals to be localized and predominately uninvolved in bonding. For the Pu(III) borates, a Pu 6p orbital is observed with delocalized electron density on basal oxygen atoms contrasting the Am(III) and Cm(III) borates, where a basal O 2p orbital delocalizes to the An 6d orbital. The electronic structure of the Ce(III) borate is similar to the Pu(III) complexes in that the Ce 4f orbital is localized and noninteracting, but the Ce 5p orbital shows no interaction with the coordinating ligands. Natural bond orbital and natural population analyses at the DFT level illustrate distinctive larger Pu 5f atomic occupancy relative to Am and Cm 5f, as well as unique involvement and occupancy of the An 6d orbitals.

■ INTRODUCTION

The similarities between the trivalent lanthanides and actinides is ascribed to the fact that their valence 4f and 5f orbitals are primarily nonbonding, and these Ln^{3+} and An^{3+} cations can possess nearly identical ionic radii that both follow the well-established contractions across the series.[1,2] This ostensibly identical chemistry has been developed in great detail for the aqua ions, for example, $[Ln(H_2O)_9]^{3+}$ and $[An(H_2O)_9]^{3+}$, where both theory and experiment confirm that the structures are isotypic, the f-orbitals are nonbonding, and the only changes that are observed occur as function of the ionic radius of the metal ions.[3] The correlations between the chemistries of these two series creates a significant technological hurdle in the recycling of used nuclear fuel where it is necessary to separate trivalent lanthanide fission products that can act as neutron poisons from Am^{3+} and Cm^{3+}; the latter can be recycled and utilized for energy production or fissioned for waste mitigation.[4]

Borates are among the most structurally complex polymeric networks known. Their structures can change as a function of numerous variables that include pH, temperature, stoichiometry, and complexation to metal ions. We have been investigating the use of molten boric acid as a reactive flux for synthesizing unusual actinide borates for the past several years. These studies have uncovered a cationic framework material with remarkable anion-exchange properties for thorium,[5] rich acentric topologies for uranium,[6] mixed-valency with neptunium,[6e−g,7] and new coordination chemistry for plutonium,[6e,g,8,9] americium,[9] and curium.[10] We have issued two communications on the structures and spectroscopy of Pu(III), Am(III), and Cm(III) borates.[9,10] These reports demonstrate that these neighboring trivalent actinides do not

Received: April 27, 2012
Published: May 29, 2012

Table 1. Crystallographic Data for $La[B_4O_6(OH)_2Cl]$ (LaBOCl), $Ce[B_4O_6(OH)_2Cl]$ (CeBOCl), $Sm_4[B_{18}O_{25}(OH)_{13}Cl_3]$ (SmBOCl), $Eu_4[B_{18}O_{25}(OH)_{13}Cl_3]$ (EuBOCl), and $Y[B_6O_9(OH)_3]$ (YBO)

compound	LaBOCl	CeBOCl	SmBOCl	EuBOCl	YBO
Mass	345.60	346.81	1510.37	1516.81	345.77
Color and habit	Colorless, Tablet	Colorless, Tablet	Colorless, Acicular	Colorless, Acicular	Colorless, Block
Space group	*Cc*	*Cc*	*P*2/*c*	*P*2/*c*	*R*3*c*
a (Å)	6.5109(4)	6.5079(9)	10.448(3)	10.4397(3)	8.346(19)
b (Å)	11.2402(6)	11.2082(16)	6.4192(18)	6.4189(2)	8.346(19)
c (Å)	9.7941(5)	9.7133(14)	23.051(6)	23.0367(6)	20.58(8)
α (deg)	90	90	90	90	90
β (deg)	105.228(3)	105.250(7)	97.220(3)	97.196(2)	90
γ (deg)	90	90	90	90	120
V (Å^3)	691.60(7)	683.56(17)	1533.7(7)	1531.56(8)	1242(7)
Z	4	4	2	2	6
T (K)	296(2)	100(2)	100(2)	296(2)	100(2)
λ (Å)	0.71073	0.71073	0.71073	0.71073	0.71073
Maximum 2θ (deg)	30.18	30.03	27.44	27.53	27.54
ρ calcd (g cm^{-3})	3.319	3.370	3.270	3.289	2.775
μ(Mo Kα)	65.73	70.60	79.53	84.86	71.18
$R(F)$ for $F_o{}^2 > 2\sigma(F_o{}^2)$[a]	0.0166	0.0167	0.0398	0.0288	0.0273
$Rw(F_o{}^2)$[b]	0.0353	0.0418	0.0930	0.0574	0.0626

[a] $R(F) = \sum||F_0| - |F_c||/\sum|F_0|$. [b] $R(F_0^2) = [\sum w(F_0^2 - F_c^2)^2/\sum w(F_0^4)]^{1/2}$.

form the same compounds when reacted with boric acid under the same conditions.

Previous reports on rare earth borates have focused on preparing lanthanide borates by reacting lanthanide oxides with boric acid either as a flux[11] or under hydrothermal conditions.[12] The flux reactions yielded hexaborates, $H_3LnB_6O_{12}$ (Ln = Sm−Lu), pentaborates, $Ln[B_5O_9]$ (Ln = Sm−Lu), octaborates, $Ln[B_8O_{11}(OH)_5]$ (Ln = La−Nd), and nonaborates, $Ln[B_9O_{13}(OH)_4]\cdot H_2O$ (Ln = Pr−Eu);[11] whereas the hydrothermal syntheses afforded $Ln_2[B_6O_{10}(OH)_4]\cdot H_2O$ (Ln = Pr, Nd, Sm−Gd, Dy, Ho, and Y).[12] In this article, we report the complete lanthanide borate series that forms when chloride is also present in the reactions, and compare and contrast it with the trivalent actinide borate series. We also report the results of a computational study of the electronic structures with the aim of comparing bonding in An^{3+} species and that of a representative lanthanide, Ce^{3+}. We demonstrate that the observed differences in the compositions and structures of the lanthanide and actinide borates are a consequence of real differences in bonding and not simply a function of ionic radii changes.

■ EXPERIMENTAL SECTION

Syntheses. *$Ln[B_4O_6(OH)_2Cl]/Ln_4[B_{18}O_{25}(OH)_{13}Cl_3]/Ln[B_6O_9(OH)_3]$.* All reported lanthanide species were synthesized starting with the appropriate $LnCl_3$ and used as received without further purification. In the cases were the chloride salt was not readily available, Ln_2O_3 was treated with 5 M HCl and reduced to a residue. $LnCl_3$ (200 mg) was charged into a PTFE-lined Parr 4749 autoclave with a 23 mL internal volume and dissolved using 215 μL of deionized water. Boric acid was then added to the sample (molar ratio 15:1 in favor of boric acid). The sample was sealed and heated at 240 °C for five days followed by slow cooling to room temperature over a 2−3 day period. The resulting products were washed extensively with boiling deionized water to remove the excess boric acid.

$Pu[B_4O_6(OH)_2Cl]$ and $Pu_2[B_{13}O_{19}(OH)_5Cl_2(H_2O)_3]$. $Pu[B_4O_6(OH)_2Cl]$ and $Pu_2[B_{13}O_{19}(OH)_5Cl_2(H_2O)_3]$ were synthesized using weapons-grade (94% ^{239}Pu and 6% ^{240}Pu, along with trace amounts of the other Pu isotopes and ^{241}Am) $PuCl_3$. Anhydrous $PuCl_3$ that results from the recycling and electrorefining of plutonium metal was used as received. $PuCl_3$ (10.6 mg) was placed in a PTFE-lined Parr 4749 autoclave with a 10 mL internal volume and then transferred into an argon-filled glovebox. Argon-sparged water (30 mL) and boric acid (63 mg) were added into the autoclave. The mixture was then sealed and heated at 240 °C for seven days followed by slow cooling to room temperature over a two day period. The furnace for heating the autoclave was also inside the glovebox to prevent oxygen from re-entering the autoclave because oxygen is not excluded by PTFE. The resulting product was washed using cold water and consisted of large blue crystals of $Pu[B_4O_6(OH)_2Cl]$ (80%) and a few clusters of much smaller crystals of $Pu_2[B_{13}O_{19}(OH)_5Cl_2(H_2O)_3]$, which are lighter in color and have an acicular habit (20%). Both compounds are not air-sensitive.

$Am[B_9O_{13}(OH)_4]\cdot H_2O$. $Am[B_9O_{13}(OH)_4]\cdot H_2O$ was synthesized using $^{243}AmO_2$ as received. AmO_2 (6.6 mg) was dissolved in 5 M HCl (100 mL) in a PTFE-lined Parr 4749 autoclave with a 10 mL internal volume. The solution was dried by heating at 130 °C, ending with a yellow solid of hydrous $AmCl_3$. The autoclave was then transferred into an argon-filled glovebox, and the same procedure was followed forthwith as was done with $PuCl_3$. The resulting product consisted of large pink tablets of $Am[B_9O_{13}(OH)_4]\cdot H_2O$ as a pure phase.

$Cm_2[B_{14}O_{20}(OH)_7(H_2O)_2Cl]$. $Cm_2[B_{14}O_{20}(OH)_7(H_2O)_2Cl]$ was synthesized using $^{248}CmCl_3$ (3% ^{246}Cm) as the starting material. $CmCl_3$ (5 mg) was placed in a PTFE-lined Parr 4749 autoclave with a 10 mL internal volume and then transferred into an argon-filled glovebox. Thirty microliters of argon-sparged water and 63 mg of boric acid were added into the autoclave, and the same procedure was followed forthwith as was done with both $PuCl_3$ and $AmCl_3$ species above. The resulting product was washed with boiling water and consisted of very pale yellow tablets of $Cm_2[B_{14}O_{20}(OH)_7(H_2O)_2Cl]$ as the sole product.

Caution! ^{239}Pu ($t_{1/2} = 2.411 \times 10^4$ y), ^{243}Am ($t_{1/2} = 7.38 \times 10^3$ y), and ^{248}Cm ($t_{1/2} = 3.48 \times 10^5$ y) all represent a serious health risk owing to their α and γ emission and the emission of their daughters. Weapons grade ^{239}Pu decays to ^{235}U ($t_{1/2} = 7.04 \times 10^8$ y) and contains ^{240}Pu ($t_{1/2} = 6.56 \times 10^3$ y) which is a potent α emitter; ^{243}Am decays to ^{239}Np ($t_{1/2}$ = 2.35 d) which is a β- and γ-emitter; ^{248}Cm decays to ^{244}Pu ($t_{1/2} = 8.08 \times 10^7$ y) as well as undergoing spontaneous fission (which accounts for approximately 8% of its decay) releasing a large flux of neutrons that can have a specific activity up to 100 mRem/h for the sample size used. All studies with plutonium, americium, and curium were conducted in a laboratory dedicated to studies on transuranium elements. This laboratory is located in a nuclear science facility and is equipped with HEPA filtered *hoods and negative pressure gloveboxes that are ported directly into the hoods. A series of counters continually monitor radiation levels in the laboratory. The laboratory is licensed by the Nuclear Regulatory Commission. All experiments were carried out with approved safety operating procedures. All free-flowing solids are worked with in gloveboxes, and products are only examined when coated with either water or Krytox oil and water. There are significant limitations in accurately determining yield with plutonium, americium, and curium compounds because this requires drying, isolating, and weighing a solid, which poses certain risks, as well as manipulation difficulties given the small quantities employed in the reactions.*

Crystallographic Studies. Crystals of all compounds were mounted on CryoLoops with Krytox oil and optically aligned on a Bruker APEXII Quazar X-ray diffractometer using a digital camera. Crystals of the transuranium compounds are glued to the CryoLoops. Initial intensity measurements were performed using a IμS X-ray source, a 30 W microfocused sealed tube (Mo Kα, λ = 0.71073 Å) with high-brilliance and high-performance focusing Quazar multilayer optics. Standard APEXII software was used for determination of the unit cells and data collection control. The intensities of reflections of a sphere were collected by a combination of four sets of exposures (frames). Each set had a different φ angle for the crystal and each exposure covered a range of 0.5° in ω. A total of 1464 frames were collected with an exposure time per frame of 10−90 s, depending on the crystal. SAINT software was used for data integration including Lorentz and polarization corrections. Semiempirical absorption corrections were applied using the program SCALE (SADABS).[13] Selected crystallographic information is listed in Tables 1 and 2. Atomic coordinates and additional structural information are provided in the Supporting Information (CIFs).

Table 2. Crystallographic Data for $Pu[B_4O_6(OH)_2Cl]$ (**PuBOCl-1**), $Pu_2[B_{13}O_{19}(OH)_5Cl_2(H_2O)_3]$ (**PuBOCl-2**), $Am[B_9O_{13}(OH)_4]\cdot H_2O$ (**AmBO**), and $Cm_2[B_{14}O_{20}(OH)_7(H_2O)_2Cl]$ (**CmBOCl**)

compound	PuBOCl-1	PuBOCl-2	AmBO	CmBOCl
Mass	445.74	1121.53	626.35	1138.91
Color and habit	Dark blue,Block	Light blue, Acicular	Pink, Tablet	Pale yellow, Tablet
Space group	Cc	$P2_1/n$	$P2_1/n$	$P2_1/n$
a (Å)	6.491(2)	8.0522(17)	7.7030(15)	7.9561(17)
b (Å)	11.184(4)	14.568(3)	16.688(3)	14.212(3)
c (Å)	9.630(3)	9.820(2)	9.872(2)	9.836(2)
α (deg)	90	90	90	90
β (deg)	105.175(9)	90.120(2)	90.073(6)	90.013(2)
γ (deg)	90	90	90	90
V (Å^3)	674.7(4)	1151.8(4)	1269.1(4)	1112.2(4)
Z	4	2	4	2
T (K)	100(2)	100(2)	100(2)	100(2)
λ (Å)	0.71073	0.71073	0.71073	0.71073
Maximum 2θ (deg)	27.50	25.360	27.54	23.26
ρ calcd (g cm^{-3})	4.388	3.234	3.278	3.401
μ(Mo Kα)	101.76	60.29	61.60	75.37
$R(F)$ for $F_o{}^2 > 2\sigma(F_o{}^2)^a$	0.0223	0.0547	0.0143	0.0645
$Rw(F_o{}^2)^b$	0.0408	0.1284	0.0370	0.1452

$^aR(F) = \sum||F_0| - |F_c||/\sum|F_0|$. $^bR(F_0^2) = [\sum w(F_0^2 - F_c^2)^2/\sum w(F_0^4)]^{1/2}$.

UV−Vis-NIR Spectroscopy. UV−vis-NIR data were acquired from individual crystals using a Craic Technologies microspectrophotometer. Crystals were placed on quartz slides under Krytox oil, and the data were collected from 200 to 1400 nm. The exposure time was auto optimized by the Craic software. The UV−vis-NIR spectra can be seen in the Supporting Information (Figures SI 11−13).

Computational Methods. Quantum chemical calculations were performed using density functional theory (DFT)[14,15] and multiconfigurational methods followed by second-order perturbation theory (CASSCF/CASPT2)[16,17] with the aim of investigating the electronic structure of the Ce^{3+} and An^{3+} borates. The initial structures were obtained from the available experimental crystal structures of $Ce[B_4O_6(OH)_2Cl]$, **CeBOCl**; $Pu[B_4O_6(OH)_2Cl]$, **PuBOCl-1**; $Pu_2[B_{13}O_{19}(OH)_5Cl_2(H_2O)_3]$, **PuBOCl-2**; $Am[B_9O_{13}(OH)_4]\cdot H_2O$, **AmBO**, and $Cm_2[B_{14}O_{20}(OH)_7(H_2O)_2Cl]$, **CmBO** and **CmBOCl**. The models employed were individually constructed to include a single Ce^{3+} or An^{3+} metal site, the capping or basal coordinating BO_3, BO_4, Cl, or H_2O ligands, and two spheres of equatorial BO_3 and BO_4 ligands. To reduce the overall negative molecular charge of the constructed models, as well as to complete valency on the terminal oxygen atoms of the capping, basal, and equatorial BO_3 and BO_4 ligands, protons (H^+) were included. The coordinates of the models employed in the calculations are reported in the Supporting Information. Constrained geometry optimizations of the protons were performed with the lanthanide/actinide metal and BO_3/BO_4 framework kept frozen at the crystal structure geometry.

Constrained geometry optimizations were performed at the DFT level with the Perdew−Burke−Ernzerhof (PBE) exchange-correlation functional[18] and a triple-ζ valence plus polarization (def-TZVP)[19] basis set on all atoms. Quasi-relativistic pseudopotentials were used for the Ce and Pu, Am and Cm atoms with a core of 28 and 60 electrons, respectively.[19,20] Constrained geometry optimizations were performed at an energy convergence of $\Delta E_h = 10^{-6}$ and a grid size of $m = 5$. All DFT calculations were performed with the TURBOMOLE 5.10 program package.[19,21]

Single-point multiconfigurational complete active space (CASSCF)[16] calculations followed by second-order perturbation theory (CASPT2)[17] were performed at the DFT optimized geometries. Scalar relativistic effects were included using the Douglas−Kroll−Hess[22] Hamiltonian to second-order and the relativistic all electron ANO-RCC basis sets with double-ζ quality (ANO-RCC-VDZP)[23] with the following contractions: [7s6p4d2f1g] for Ce; [8s7p5d3f1g] for Pu, Am, and Cm; [4s3p1d] for Cl; and [3s2p1d] for B and O. The ANO-RCC-MB basis set was employed for H with a contraction of [1s]. CASSCF/CASPT2 calculations on the lowest possible spin states of the Ce^{3+} and An^{3+} borates were performed at the optimized DFT geometries to decisively ascertain the ground spin state. For **CeBOCl**, with a Ce $4f^1$ electronic configuration, the ground state was undoubtedly a doublet state. However, the ground electronic configuration of the An^{3+} borates was slightly more complex due to the unpaired f-electrons in **PuBOCl-1** and **PuBOCl-2**, **AmBO**, and **CmBO** and **CmBOCl** of Pu $5f^5$, Am $5f^6$, and Cm $5f^7$ where the ground spin states were sextet, septet, and octet, respectively.

The initial active spaces for **PuBOCl-1** and **PuBOCl-2**, **AmBO**, and **CmBO** and **CmBOCl** included five, six, and seven electrons in the seven 5f-orbitals, respectively. The final active space was expanded to include an additional doubly occupied and corresponding antibonding orbital. For **CeBOCl**, an initial active space included a single electron in seven 4f-orbitals; however, expanding the active space introduced virtual Ce 5d orbitals, and the final active space was restricted to include three electrons in three orbitals, the Ce 4f orbital and a doubly occupied bonding and antibonding pair. For **CeBOCl**, **PuBOCl-1**, and **PuBOCl-2**, the additional orbital corresponded to a Ce 5p and Pu 6p while for **AmBO-1**, **CmBO**, and **CmBOCl**, the An 6p orbital was lower in energy below the valence region, and an O 2p orbital of the basal BO_3/BO_4 ligand enters the active space.

The computational costs arising from the two-electron integrals were drastically reduced by employing the Cholesky decomposition (CD) technique in all CASPT2 calculations[24−26] combined with the Local Exchange (LK) screening.[27] The CASPT2 approach has been successful in studying many actinide-containing systems.[28−32] The CASSCF/CASPT2 calculations were performed with the MOLCAS 7.3 package.[33]

■ RESULTS AND DISCUSSION

Structure and Topology Description. *Lanthanides: Ln[B$_4$O$_6$(OH)$_2$Cl].* The reaction of the lanthanide/actinide chlorides and boric acid is a facile method for the production of f-element polyborate species. The early lanthanides result in the formation of Ln[B$_4$O$_6$(OH)$_2$Cl] (Ln = La–Nd), which crystallize in the noncentrosymmetric, monoclinic space group, *Cc*. The praseodymium and neodymium species have previously been reported,[34] but the lanthanum (**LaBOCl**) and cerium (**CeBOCl**) analogues are a result of this work.

$$\mathrm{LnCl_3(s) + 4H_3BO_3(s) \rightarrow Ln[B_4O_6(OH)_2Cl](s) + 4H_2O(l) + 2HCl(g)} \quad (\mathrm{Ln = La{-}Nd}) \qquad (1)$$

These compounds form dense, three-dimensional structures as shown in Figure 1a and contain only corner-sharing BO$_3$ and BO$_4$ units, which create triangular holes (comprised of two BO$_4$ tetrahedra and one BO$_3$ triangle) where the lanthanide cations reside. The sheet topology (Figure 1b) found in these species is very similar to those found with penta- and hexavalent actinides (e.g., U(VI), Np(V), Np(VI), and Pu(VI)).[6−8]

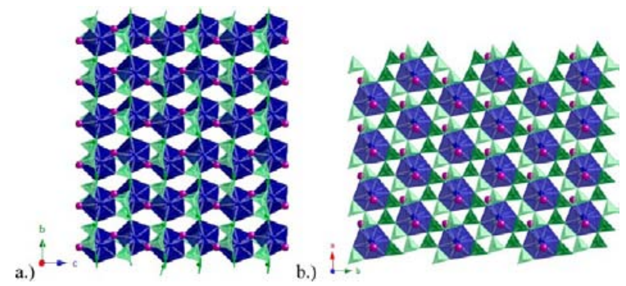

Figure 1. Depiction of the (a) three-dimensional framework and (b) sheet topology of Ln[B$_4$O$_6$(OH)$_2$Cl] (Ln = La–Nd; Pu). The lanthanide and plutonium metal centers are depicted by the blue spheres, chlorine is depicted by the purple spheres, BO$_4$ tetrahedra as light green unit, and BO$_3$ triangles as dark green units.

The polyborate sheet topology provides six oxygen donors that are nearly co-planar forcing a 10-coordinate geometry not typically found for trivalent lanthanides or actinides. This 10-coordinate geometry (Figure 2a) is best described as a capped triangular cupola,[35] where the capping group is a chloride anion, and the triangular base is composed of oxygen atoms from two different BO$_4$ groups and an additional chloride anion. Furthermore, both chloride anions bridge between metal centers, and these bridges span between the sheets. This type of connectivity is absent in nearly all of the lanthanide and actinide borates that have been prepared.

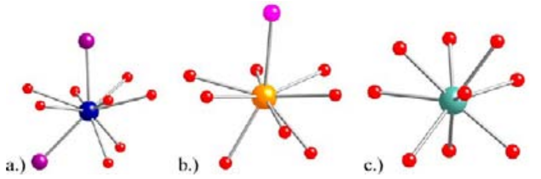

Figure 2. Coordination geometries for the lanthanide and actinide metal centers. (a) Capped triangular cupola, (b) hula hoop, (c) tricapped trigonal prism.

The equatorial oxygen bond lengths in **LaBOCl** range from 2.586(3) to 2.733(3) Å while the base bond lengths are 2.501(3) and 2.553(2) Å (Table SI 7). The equatorial oxygen bond lengths in **CeBOCl** range from 2.575(3) to 2.724(3) Å while the base bond lengths are 2.477(3) and 2.529(3) Å (Table SI 7). The capping chlorides have distances of 2.9247(9) and 2.8939(11) Å for **LaBOCl** and **CeBOCl**, respectively. The additional base chloride has bond lengths of 2.9265(9) and 2.9127(10) Å for **LaBOCl** and **CeBOCl**, respectively. Both chloride anions bridge between the metal centers, and these bridges span between the sheets (Figure 1a). The bond distances for the Pr and Nd analogues have been reported elsewhere.[34]

Ln$_4$[B$_{18}$O$_{25}$(OH)$_{13}$Cl$_3$]. Samarium and europium both represent a transition point in the lanthanide series. The product obtained from these lanthanides is Ln$_4$[B$_{18}$O$_{25}$(OH)$_{13}$Cl$_3$] (Ln = Sm, Eu; **SmBOCl** and **EuBOCl**), which crystallize in the centrosymmetric, monoclinic space group, *P*2/*c*.

$$\mathrm{8LnCl_3(s) + 36H_3BO_3(s) \rightarrow 2Ln_4[B_{18}O_{25}(OH)_{13}Cl_3](s) + 32H_2O(l) + 18HCl(g)} \quad (\mathrm{Ln = Sm{-}Eu}) \qquad (2)$$

These compounds also form dense but different, three-dimensional structures (Figure 3a), as well as a different sheet topology (Figure 3b). Like **LaBOCl** and **CeBOCl**, corner-sharing BO$_3$ and BO$_4$ units create triangular holes (also comprised of two BO$_4$ tetrahedra and one BO$_3$ triangle), which provide residence for the metal center. The Ln$_4$[B$_{18}$O$_{25}$(OH)$_{13}$Cl$_3$] product is novel not only for the lanthanides, but also for the actinides.

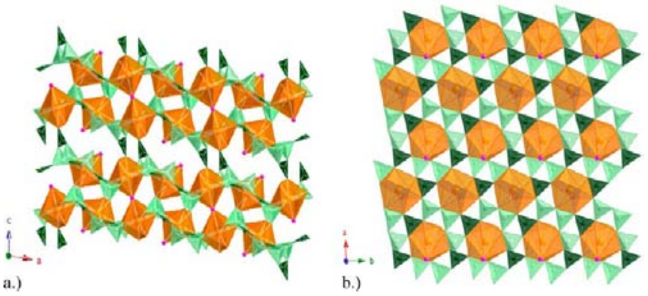

Figure 3. Depiction of the (a) three-dimensional framework and (b) sheet topology of Ln$_4$[B$_{18}$O$_{25}$(OH)$_{13}$Cl$_3$]; Ln = Sm, Eu. The lanthanide metal centers are depicted by the orange spheres, chlorine is depicted by the purple spheres, BO$_4$ tetrahedra as light green unit, and BO$_3$ triangles as dark green units.

The metal centers in this structure are either bridged or terminal, but all possess an unusual nine-coordinate hula-hoop geometry (Figure 4a).[36] Like the **LaBOCl** and **CeBOCl** structure, the polyborate network provides six oxygen atoms that are nearly co-planar, and the additional ligands are two additional oxygens from either two BO$_4$ groups (bridged compounds) or one oxygen from a BO$_3$ group and a hydroxide (nonbridged compounds). This chloride bridge is similar to what is observed in Ln[B$_4$O$_6$(OH)$_2$Cl] (Ln = La–Nd) though **SmBOCl** and **EuBOCl** contain only one bridging, apical chloride.

The Ln–Cl bond lengths in the bridged **SmBOCl** and **EuBOCl** metal centers are 2.7571(8) and 2.7500(3) Å, respectively, while the unbridged metal centers possess Ln–Cl bond lengths of 2.746(2) and 2.7318(15) Å. The equatorial bond lengths range from 2.468(5) to 2.693(5) Å and 2.461(4) to 2.693(4) Å and base lengths of 2.392(6) and 2.457(5) Å and

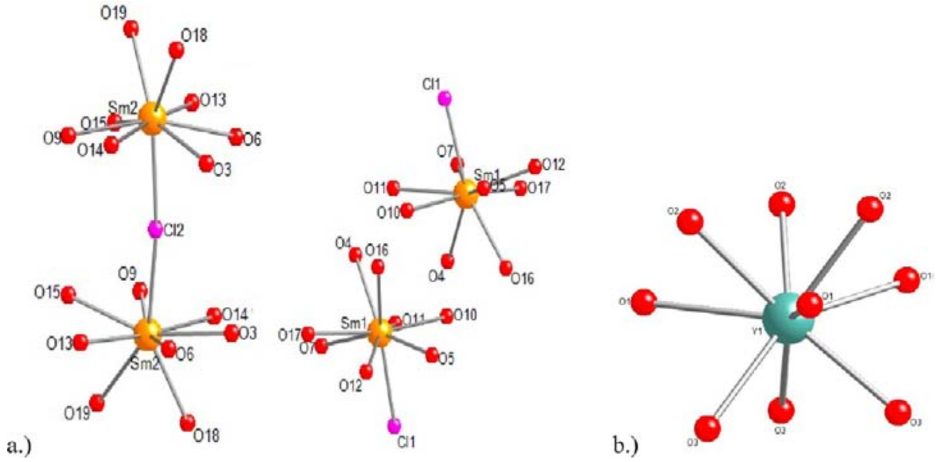

Figure 4. Coordination geometries and labeled bonds in (a) $Ln_4[B_{18}O_{25}(OH)_{13}Cl_3]$, Ln = Sm, Eu; and (b) $Ln[B_6O_9(OH)_3]$, Ln = Eu−Lu, Y. The lanthanide metal center is depicted by orange (a) or gray (b), oxygens as red spheres, and chlorine as purple spheres.

2.381(4) and 2.444(4) Å in the bridged **SmBOCl** and **EuBOCl** metal centers, respectively. The unbridged metal centers have equatorial bond lengths of 2.435(5) to 2.564(5) Å and 2.429(3) to 2.574(4) Å and base lengths of 2.462(5) and 2.464(5) Å and 2.452(4) and 2.453(4) Å for **SmBOCl** and **EuBOCl**, respectively (Table SI 8).

$Ln[B_6O_9(OH)_3]$. The structure and local coordination environment of $Ln[B_6O_9(OH)_3]$ (Ln = Y, Eu−Lu) has been reported elsewhere[11a,b] and are shown in Figures 4b and 5.

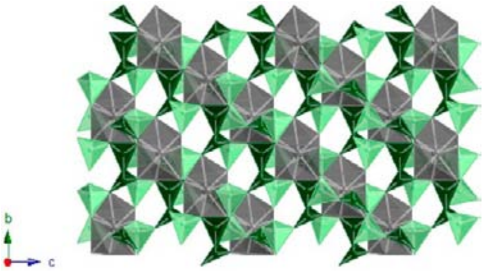

Figure 5. Depiction of the three-dimensional framework of $Ln[B_6O_9(OH)_3]$; Ln = Eu−Lu, Y. The lanthanide metal center is depicted by the gray spheres, BO_4 tetrahedra as light green units, and BO_3 triangles as dark green units.

However, this study has found that yttrium, which is generally regarded as an honorary lanthanide, forms the $Ln[B_6O_9(OH)_3]$ structure type as well (**YBO**). It should be noted that, due to the exclusion of chloride from the inner coordination sphere, a change in geometry to a more typical tricapped trigonal prism, and crystallization in the rhombohedral space group, *R*3*c*, is observed with the smaller lanthanides.

$$2LnCl_3(s) + 12H_3BO_3(s) \rightarrow 2Ln[B_6O_9(OH)_3](s) + 12H_2O(l) + 6HCl(g) \quad (Ln = Y, Eu{-}Lu) \tag{3}$$

Table SI 9 shows the Y−O bond distances present in **YBO**. The apical Y−O bond distances are 2.347(6) and 2.339(6) Å for O2 and O3, respectively, while the capping bond (O1) distance is 2.447(6) Å.

Actinides: $Pu[B_4O_6(OH)_2Cl]$. As the redox chemistry for plutonium is more complex than any of the lanthanides, strict anaerobic conditions are required in order to obtain trivalent plutonium borates. When obtained, plutonium produces two different products. The first and major product (80%), $Pu[B_4O_6(OH)_2Cl]$ (**PuBOCl-1**), is isotypic with the **LaBOCl** and **CeBOCl** compounds.

$$PuCl_3(s) + 4H_3BO_3(s) \rightarrow Pu[B_4O_6(OH)_2Cl](s) + 4H_2O(l) + 2HCl(g) \tag{4}$$

The structure, sheet topology, and local coordination environment discussions are mentioned above and can be seen in Figures 1 and 2a. Selected bond lengths are given in Table SI 10. The equatorial bond lengths range from 2.574(5) to 2.722(5) Å, base bond lengths are 2.445(5) and 2.500(5) Å, the apical chloride has a bond length of 2.862(2) Å, and the base chloride has a bond length of 2.891(2) Å.

$Pu_2[B_{13}O_{19}(OH)_5Cl_2(H_2O)_3]$. The second trivalent plutonium borate, $Pu_2[B_{13}O_{19}(OH)_5Cl_2(H_2O)_3]$ (**PuBOCl-2**), is the minor product (20%) of the reaction and is completely novel for the lanthanides and actinides. $Pu_2[B_{13}O_{19}(OH)_5Cl_2(H_2O)_3]$ crystallizes in the centrosymmetric, monoclinic space group $P2_1/n$ and does not have a lanthanide analogue.

$$2PuCl_3(s) + 13H_3BO_3(s) \rightarrow Pu_2[B_{13}O_{19}(OH)_5Cl_2(H_2O)_3](s) + 12H_2O(l) + 4HCl(g) \tag{5}$$

The three-dimensional framework, local coordination environment, and sheet topology (Figures 6, 7a, and 8a) of **PuBOCl-2** are completely different than those of **LaBOCl**, **CeBOCl**, or **PuBOCl-1**. **PuBOCl-2** is a 10-coordinate environment with the capped triangular cupola geometry (Figure 7a).

The polyborate network provides six oxygen atoms that are nearly co-planar, and the additional ligands are a capping chloride and a triangular base composed of a water molecule and oxygen atoms from two different BO_3 groups. The apical chloride in this compound is terminal and does not bridge to other metal centers. While triangular holes are still present in the sheet topology, the units making up the holes are two BO_3 triangles and one BO_4 tetrahedra. This is the complete opposite of what is seen in **LaBOCl**, **CeBOCl**, and **PuBOCl-1**. Additionally, the sheet topology contains a unit of three corner sharing BO_4 tetrahedra connected via a μ_3-oxygen. For comparison, this sheet topology is also present in the

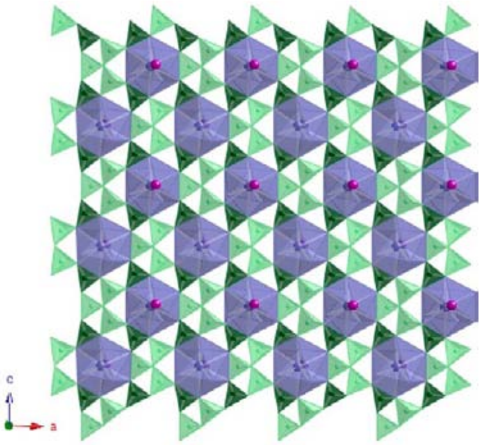

Figure 6. Depiction of the sheet topology in $Pu_2[B_{13}O_{19}(OH)_5Cl_2(H_2O)_3]$, $Am[B_9O_{13}(OH)_4]\cdot H_2O$, and $Cm_2[B_{14}O_{20}(OH)_7(H_2O)_2Cl]$. The actinide metal centers are depicted by the blue spheres, chlorine is depicted by the purple spheres, BO_4 tetrahedra as light green unit, and BO_3 triangles as dark green units. The chlorine is absent in the $Am[B_9O_{13}(OH)_4]\cdot H_2O$ sheet topology.

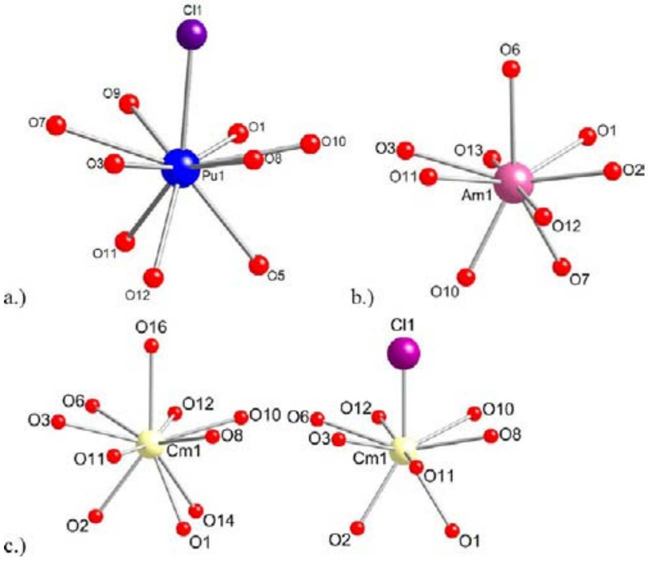

Figure 7. Coordination geometries and labeled bonds in (a) $Pu_2[B_{13}O_{19}(OH)_5Cl_2(H_2O)_3]$, (b) $Am[B_9O_{13}(OH)_4]\cdot H_2O$, and (c) $Cm_2[B_{14}O_{20}(OH)_7(H_2O)_2Cl]$. The actinide metal centers are depicted by blue (a), pink (b), or yellow (c) spheres, oxygens as red spheres, and chlorine as purple spheres.

$Ln[B_8O_{11}(OH)_5]$ (Ln = La–Nd) and $Ln[B_9O_{13}(OH_4)]\cdot H_2O$ (Ln = Pr–Eu) systems,[11c] but the three-dimensional framework is novel. Selected bond lengths are given in Table SI 11. The equatorial bond lengths range from 2.536(10) to 2.726(11) Å, base bond lengths ranging from 2.471(18) to 2.614(12) Å, and the capping chloride has a bond length of 2.753(5) Å.

$Am[B_9O_{13}(OH)_4]\cdot H_2O$. The americium borate, $Am[B_9O_{13}(OH)_4]\cdot H_2O$ (**AmBO**), represents a transition in the actinide series as far as structure, coordination environment, and bonding is concerned. While **AmBO** crystallizes in the monoclinic space group $P2_1/n$ and has the same sheet topology as **PuBOCl-2,** without the chloride moiety (Figure 6), its local coordination environment and three-dimensional network are completely different (Figures 7b and 8b). The most noticeable difference between **AmBO**, **PuBOCl-1**, and **PuBOCl-2** is the lack of chloride.

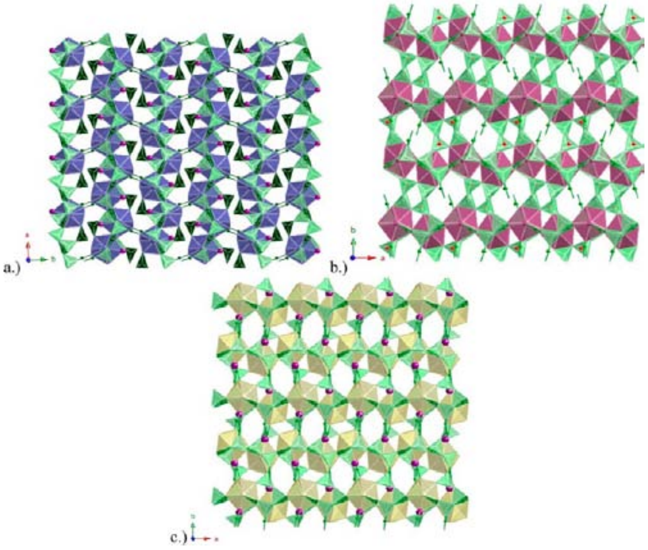

Figure 8. Depiction of the three-dimensional framework in (a) $Pu_2[B_{13}O_{19}(OH)_5Cl_2(H_2O)_3]$, (b) $Am[B_9O_{13}(OH)_4]\cdot H_2O$, and (c) $Cm_2[B_{14}O_{20}(OH)_7(H_2O)_2Cl$. The actinide metal centers are depicted by blue (a), pink (b), or yellow (c) spheres, BO_4 tetrahedra as light green unit, and BO_3 triangles as dark green units.

$$2AmCl_3(s) + 18H_3BO_3(s) \rightarrow 2Am[B_9O_{13}(OH)_4]\cdot H_2O(s) + 18H_2O(l) + 6HCl(g) \tag{6}$$

AmBO has the same nine-coordinate hula-hoop geometry (Figure 7b) as observed in the **SmBOCl** and **EuBOCl** structures. The six nearly co-planar equatorial oxygen atoms come from two BO_3 triangles and one BO_4 tetrahedra present in the sheet layer and create the triangular hole in which the americium atom resides. The additional oxygen atoms come from one chelating BO_4 tetrahedron in the base and one BO_3 triangle in the capping position, which bridges to the layer above. Selected bond lengths can be seen in Table SI 12. The equatorial bond lengths range from 2.470(2) to 2.614(2) Å, base bond lengths of 2.356(2) and 2.431(2) Å, and a capping oxygen with a bond length of 2.582(2) Å.

$Cm_2[B_{14}O_{20}(OH)_7(H_2O)_2Cl]$. The curium borate, $Cm_2[B_{14}O_{20}(OH)_7(H_2O)_2Cl]$ (**CmBOCl**), is a unique structure in that it contains two distinct curium sites with different coordination geometries and is novel for both the lanthanides and actinides. The first site is a 10-coordinate capped triangular cupola with an oxygen in the capping position, and the second is a nine-coordinate hula-hoop with a terminal chloride in the apical position (Figure 7c). **CmBOCl** crystallizes in the monoclinic space group $P2_1/n$ and has the same sheet topolgy as **PuBOCl-2** and **AmBO** (Figure 6), but a completely different three-dimensional framework (Figure 8c). It is interesting to note the renewal of the chloride moiety even if on only half the curium sites.

$$2CmCl_3(s) + 14H_3BO_3(s) \rightarrow Cm_2[B_{14}O_{20}(OH)_7(H_2O)_2Cl](s) + 13H_2O(l) + 5HCl(g) \tag{7}$$

The 10-coordinate center in **CmBOCl** is capped by an oxygen atom from a BO_3 triangle, and the triangular base is composed of oxygen atoms from one BO_3 group and two different BO_4 groups. The nine-coordinate center has a chloride as the capping group, and the two base sites are composed of oxygen atoms from two different BO_4 groups. Select bond lengths are given in Table SI 13. The 10-coordinate center has equatorial bond lengths ranging from 2.531(14) to 2.686(15) Å, base bond lengths ranging from 2.457(17) to 2.760(3) Å, and a capping oxygen bond length of 2.684(3) Å. The nine-coordinate center has equatorial bond lengths ranging from 2.531(14) to 2.686(15) Å, base bond lengths of 2.457(17) and 2.530(3) Å, and a capping chloride bond length of 2.685(11) Å. While **PuBOCl-2**, **AmBO**, and **CmBOCl** all crystallize in the same space group, it is the differing connectivities between their respective sheets as well as differing capping and base moieties that lead to the variation observed in their three-dimensional frameworks. In **AmBO** and **CmBOCl**, both BO_3 triangles and BO_4 tetrahedra connect the sheets together, while **PuBOCl-2** has only BO_3 triangles connecting the sheets together.

Periodic Trends. From this study, it became evident that there are discontinuities in the resulting structure types that occur between the lanthanide and actinide borates. The lanthanides yield products that occur in blocks that depend on (a) the presence/absence of the chloride and (b) steric factors that correlate with changes in the ionic radii of these elements. Depending on the identity of the lanthanide, three different products were obtained in high yield, which can be seen in eqs 1−3.

It is unfortunate that the ionic radii for Pu^{3+} and Cm^{3+} have never been determined beyond coordination number (CN) six and Am^{3+} beyond eight.[2] Thus, the highest value common between the lanthanides and actinides is six and will be used for comparisons henceforth. The first structure type that emerges from the lanthanides is $Ln[B_4O_6(OH)_2Cl]$ (Ln = La−Nd) where the trivalent ionic radii for these metals are 1.032, 1.01, 0.99, and 0.98 Å, respectively.[2] The second structure type, $Ln_4[B_{18}O_{25}(OH)_{13}Cl_3]$ (Ln = Sm, Eu), possess metal centers with trivalent ionic radii of 0.958 and 0.947 Å, respectively, while the third structure type, which lacks the chloride entirely, $Ln[B_6O_9(OH)_3]$ (Ln = Y, Eu−Lu), possess metal centers with trivalent ionic radii of 0.947 to 0.861 Å, respectively.[2] It is of interest that yttrium belongs in the third structure type. With a trivalent ionic radius (CN = 6) of 0.900 Å, yttrium would fall roughly in between holmium and erbium.[2]

The actinide products, however, do not seem to depend on the presence/absence of chloride or the ionic radii, but instead on the identity of the metal itself. Depending on the identity of the actinide, four different products were obtained and can be seen in eqs 4−7.

The ionic radii (CN = 6) for Pu^{3+}, Am^{3+}, and Cm^{3+} are 1.00, 0.975, and 0.970 Å, respectively.[2] Upon examination of the ionic radii, it would be expected, based solely upon purely ionic interactions, that plutonium should yield exclusively the $Ln[B_4O_6(OH)_2Cl]$ compound and americium and curium should yield the same compound yet different than any of the lanthanide products . However, this expectation is not entirely realized. While the plutonium does indeed yield **PuBOCl-1**, which is isotypic with the **LaBOCl** product, it also produces a minor product of **PuBOCl-2** which is not observed in any of the lanthanide reactions or for any other actinide reaction to date.[9,10] **AmBO** lacks chloride entirely and is isotypic with the products obtained where the lanthanide oxides of Pr and Nd−Eu are used as the starting material.[11a,b] The curium reaction, which was expected to yield the same product as the americium based solely on the ionic radii, produced $Cm_2[B_{14}O_{20}(OH)_7(H_2O)_2Cl]$ with two different curium sites.[10] The first site possesses a nine-coordinate geometry and contains a chloride, while the other site lacks the chloride but is 10-coordinate. This is a hybrid of what is observed in the plutonium and americium reactions. Also, this product, to date, is unique only to curium. It is of interest that the area of greatest structural change occurs for the congeners of each series (Sm−Gd for the lanthanides and Pu−Cm for the actinides). It should be noted that several different lanthanide to boric acid molar ratios (ranging from 1:15 to 1:60), as well as variations in temperature (ranging from 200 to 240 °C) were investigated in which the same products presented above were obtained. The only difference that occurred was that by using a molar ratio of 1:60 in favor of boric acid, only one europium compound ($Eu[B_6O_9(OH)_3]$) was obtained. As such, we think that **PuBOCl-2** and **CmBOCl** are completely novel and exclusive to the actinides.

The average bond length in **AmBO** is 2.497 Å while the averages for **PuBOCl-1** and **PuBOCl-2** are 2.585 and 2.609 Å, respectively. This large difference in An−O bond lengths between the plutonium and americium borates can be attributed to a change in coordination environment, different structures, as well as a substantial change in ionic radii. The average bond length in **CmBOCl** is 2.557 and 2.590 Å for the 9- and 10-coordinate species, respectively. These averages fall roughly in the middle of what is observed in **PuBOCl-1**, **PuBOCl-2**, and **AmBO**, which is to be expected as **CmBOCl** has bonding and coordination environments of both the plutonium and americium borates.

Under the Pearson definition of hard/soft acids and bases, the lanthanides and actinides are considered hard acids while chloride is a soft base.[37] This line of thought nicely explains the trend of all bridging, to half bridging, to the absence of chloride entirely as the lanthanide series is traversed. However, it is less direct for the actinides. A typical change in ionic radius for adjacent actinides in the same oxidation state with the same coordination number is approximately 0.01 Å.[2] As the change in ionic radius is larger than one would expect between plutonium and americium, it is not entirely surprising that americium would elect to exclude chloride from the inner coordination sphere. Furthermore, it does not explain the renewal of the chloride moiety in the curium structure where the curium is smaller and slightly “harder” than americium. It appears that the notion of ionic and steric factors as the largest contributors to the products of the f-block elements may not be entirely true for the actinides, and other factors such as an increased involvement of the 5f/6d orbitals as well as the metal itself must be considered.

Absorption Spectroscopy. The absorption spectra for **PuBOCl-1**, **PuBOCl-2**, **AmBO**, and **CmBOCl** were obtained using a microspectrophotometer and are shown in the Supporting Information (Figures SI 11−13). The ground states of Pu^{3+} and Am^{3+} are $^6H_{5/2}$ and $^7F_0$, respectively. The ground state for Cm^{3+} is more complicated. The ground state for Cm^{3+} is only 87% $^8S_{7/2}$ as spin−orbit coupling mixes in substantial contributions from $^6P_{7/2}$, $^6D_{7/2}$, and higher terms, resulting in crystal-field splittings of about 5−100 cm^{-1}.[38] The spectra of each display a vast series of Laporte forbidden f−f transitions throughout the UV−vis-near IR region. These f−f transitions have been carefully assigned by Carnall and co-

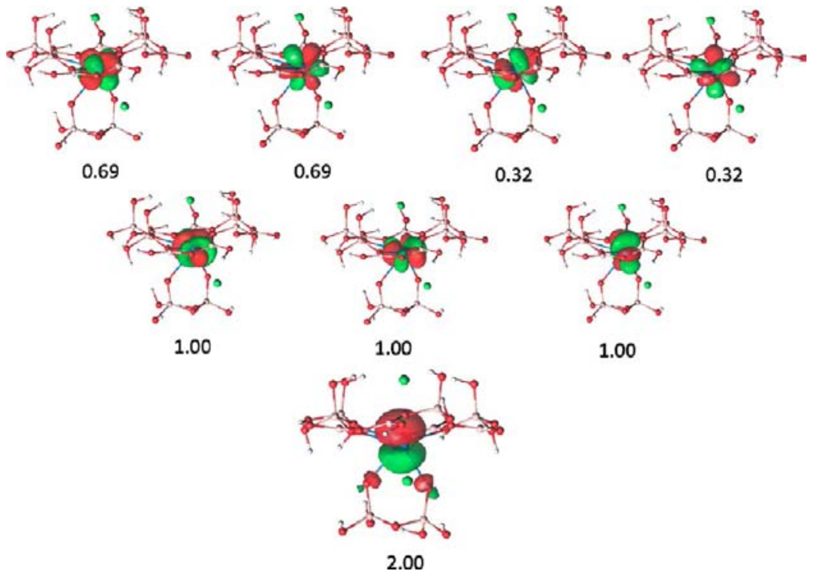

Figure 9. Selected molecular orbitals responsible for the bonding in **PuBOCl-1** at the CASSCF level. Respective occupation numbers are indicated below the orbital plots (isovalue 0.04). Pu, blue; Cl, bright green; O, red; B, light pink; and H, white.

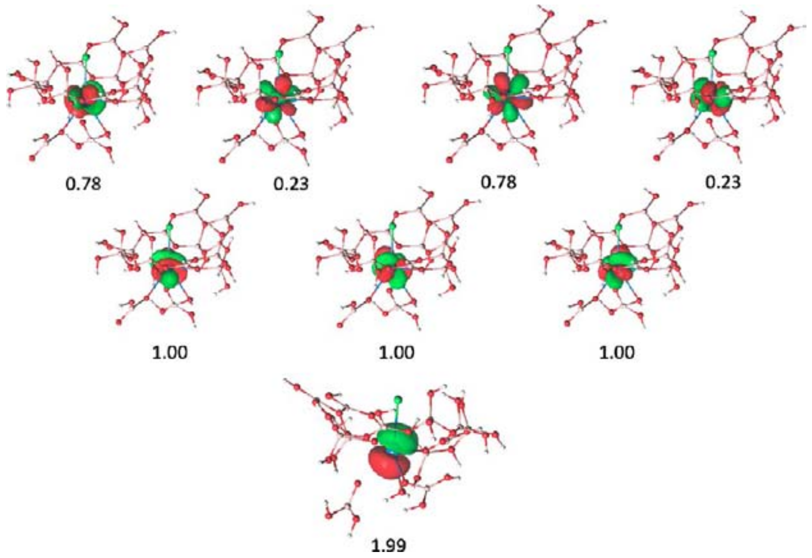

Figure 10. Selected molecular orbitals responsible for the bonding in **PuBOCl-2** at the CASSCF level. Respective occupation numbers are indicated below the orbital plots (isovalue 0.04). Pu, blue; Cl, bright green; O, red; B, light pink; and H, white.

workers,[39] and we have used this analysis to assign the transitions shown.

The most important transitions that occur for Pu^{3+} are the $^6H_{5/2} \rightarrow {}^6H_{13/2}$ transitions near 900 nm. Fortunately, this region is bare for Pu^{4+}. The $^4L_{13/2}$ and $^4M_{15/2}$ transitions are also routinely used to identify Pu^{3+}. The most important transitions that occur for Am^{3+} are the $^7F_0 \rightarrow {}^5L_6$ transition near 500 nm and the $^7F_0 \rightarrow {}^7F_6$ transition near 800 nm. While the chemistry of curium is overwhelmingly dominated by the trivalent state, the $^8S_{7/2} \rightarrow 0.88\ {}^6I + 0.26\ {}^4K_2$ and $^8S_{7/2} \rightarrow 0.64\ {}^6I + 0.32\ {}^4H_2$ can be used as diagnostic transitions as these are not present in the spectrum of Cm^{4+}. It is important to note that for the actinides, the absorption spectrum can be a powerful tool in determination of the oxidation state even when substantially different coordination geometries are observed.

Electronic Structure Calculations. Insights into the role of the 5f and 4f orbitals in bonding were obtained through electronic structure analyses at the CASSCF and DFT levels where selected molecular orbitals in the HOMO−LUMO region involving the 5f and 4f orbitals are depicted in Figures 9 and 10 and Figures SI 1−10, respectively.

In terms of relative state energies, the quartet states of **PuBOCl-1** and **PuBOCl-2** were predicted to be an average of 45 kcal/mol above the sextet state while the quintet state of **AmBO** was 47 kcal/mol above the septet state at the CASPT2 level. With a Cm $5f^7$ electronic configuration, the half-filled f-orbitals afford significant stability and the sextet states of **CmBO** and **CmBOCl** are an average of 97 kcal/mol above the octet state.

The active space for **PuBOCl-1** and **PuBOCl-2**, **AmBO**, and **CmBO** and **CmBOCl** included five, six, and seven electrons in seven 5f orbitals and an additional doubly occupied orbital, respectively, and, irrespective of structure and actinide metal, the 5f orbitals are all localized on the metal site (Figures 9 and

10 and Figures SI 1−4) with no evident interaction with any coordinating atoms. However, a unique orbital picture is depicted just below the valence 5f orbitals. For **PuBOCl-1**, a Pu 6p orbital shows delocalization of electron density to a basal O 2p orbital (Figure 9), while for **PuBOCl-2**, the Pu 6p orbital is localized and shows no interaction (Figure 10). For **AmBO**, immediately below the valence Am 5f orbitals, a basal O 2p orbital shows delocalization of electron density to an Am 6d orbital (Figure SI 1). Unlike the Pu structures, the Am 6p orbital lies outside of the active pace and is lower in energy than the Am 5f orbitals. As seen in **AmBO**, a basal O 2p orbital in **CmBO** and **CmBOCl** is delocalized toward a Cm 6d orbital (Figures SI 2 and 3). Additional electronic structure analyses performed at the PBE level confirm localization of the highest singly occupied alpha spin molecular 5f orbitals (SOMOs) (Figures SI 5−10) and is discussed further in the Supporting Information.

For **CeBOCl**, a single Ce 4f orbital is localized on the metal site without any interaction to the coordinating ligands. This orbital picture is similar to that observed for the An^{3+} borates where all the An 5f orbitals were localized. Just below the Ce 4f SOMO, an analogous Ce 5p orbital is observed as in **PuBOCl-1**, but without any interaction to coordinating atoms (Figure SI 4).

Additional insights into the electronic structure of the An^{3+} borates were obtained from natural bond orbital (NBO) and natural population (NPA) analyses. At the CASSCF level, Mülliken and LoProp methods predicted similar atomic charges on the actinide metal irrespective of structure (Table 3), with the former on average 0.3e less than LoProp. Similarly, partial atomic charges were predicted at the DFT level, and the NPA charges (Table 3) were further away from the ideal +3 oxidation state than the CASSCF values. The natural charges on Pu were predicted to be less than Am by ∼0.44e and Cm by an average of ∼0.42e, indicating a larger transfer of electron density from coordinating oxygens to the actinide metal in **PuBOCl-1** and **PuBOCl-2** than in **AmBO**, **CmBO**, and **CmBOCl**.

Table 3. Mülliken, LoProp, and Natural Population Analysis Atomic Charges and Mülliken Spin Population Per Lanthanide or Actinide Metal at the CASSCF/ANO-RCC-PVDZ and DFT-PBE/def-TZVP Levels

	CASSCF			PBE
molecule	Mülliken atomic charges	Mülliken spin population	LoProp atomic charges	natural population atomic charges
CeBOCl	2.08	1.00	2.43	1.53
PuBOCl-1	2.07	4.98	2.42	1.29
PuBOCl-2	2.18	4.98	2.49	1.30
AmBO	2.14	5.98	2.47	1.73
CmBO	2.19	6.98	2.52	1.77
CmBOCl	2.08	6.98	2.48	1.67

Furthermore, NPA electronic configurations revealed a unique involvement of the An 5f and An 6d orbitals. Considering the An 5f electronic configurations, **PuBOCl-1** **5f$^{5.35}$** and **PuBOCl-2** **5f$^{5.51}$** show a larger relative electron occupation compared to **AmBO** 5f$^{6.22}$, **CmBO** 5f$^{7.19}$, and **CmBOCl** 5f$^{7.17}$, indicating a larger transfer of electron density to Pu (Table SI 2). This is consistent with the ionic contraction in going from Pu^{3+} to Am^{3+} to Cm^{3+} and the expected localization and decreased involvement of the Am and Cm 5f orbitals. The electronic configurations of **PuBOCl-1** 6d$^{1.02}$ and **PuBOCl-2** 6d$^{0.90}$ reveal larger electron occupation compared to Am and Cm 6d by ∼0.1e (Table SI 1).

Additionally, total and decomposed atomic populations from the total density were predicted using Loewdin and NPA methods (Table 4 and Table SI 2), where those of the latter will be used in the discussion below. Irrespective of structure and actinide metal, the 6s and 6p atomic populations were approximately the same for each structure. However, there was a difference in the An 5d atomic populations beyond the expected 5d^{10} configuration, being largest for **PuBOCl-1** (11.09 e) and **PuBOCl-2** (10.96 e) and indicative of a transfer of electrons from the coordinating oxygens (Table 4). Considering the An 5f orbitals, there was a similar comparative increase in atomic population of Pu 5f orbitals (**PuBOCl-1**, 5.38 e and **PuBOCl-2**, 5.54 e) compared to that of Am 5f and Cm 5f (Table 4).

Lastly, the total and decomposed atomic $(\alpha-\beta)$ spin density were also predicted employing the Loewdin and NPA methods (Table SI 4), and irrespective of method, the total $(\alpha-\beta)$ spin densities are as expected, Pu ∼5, Am ∼6, and Cm ∼7, with the largest contribution arising from the An 5f orbitals. At the CASSCF level, for **PuBOCl-1**, **PuBOCl-2**, **AmBO**, **CmBO**, and **CmBOCl**, bond orders of 1.00 (Table SI 5) are predicted between the An and basal O atoms or chloride ligands. For **CeBOCl**, bond orders are predicted between Ce and the O or Cl atoms; however, bond orders of 1.00 were also predicted between Ce and each equatorially coordinated O atom.

■ CONCLUSIONS

This work represents the first full report on lanthanide borate chlorides and their comparison to the trivalent actinide borate chlorides. The structural chemistry is largely dependent on the ionic radii of the metals, the presence or absence of the chloride anion, and the exclusion of the 4f orbitals in bonding for the lanthanides and less so for the actinides as the identity of the metal seems to be the most influential.

Table 4. Loewdin and Natural Population Analysis Atomic Populations from the Total Density at the DFT-PBE/def-TZVP Level

	Loewdin				natural population			
molecule	n(s)	n(p)	n(d)	n(f)	n(s)	n(p)	n(d)	n(f)
PuBOCl-1	4.157	12.463	11.556	5.862	4.221	12.013	11.087	5.384
PuBOCl-2	4.134	12.378	11.441	6.012	4.197	12.000	10.964	5.539
AmBO	4.100	12.302	11.413	6.646	4.178	11.998	10.860	6.231
CmBO	4.135	12.351	11.354	7.616	4.184	12.005	10.848	7.194
CmBOCl	4.154	12.424	11.479	7.617	4.200	12.004	10.847	7.182
CeBOCl	4.105	12.230	11.503	1.537	4.189	11.995	11.125	1.156

While the Ln[$B_4O_6(OH)_2Cl$] (Ln = La−Nd) compounds are isotypic with Pu[$B_4O_6(OH)_2Cl$], a secondary phase, $Pu_2[B_{13}O_{19}(OH)_5Cl_2(H_2O)_3]$, does exist which has no lanthanide analogue. However, Am[$B_9O_{13}(OH)_4$]·H_2O, which does have a lanthanide analogue, is only observed for the lanthanides when chloride is excluded entirely and is the only actinide we have studied that does not incorporate chloride in the final product. It is this Pu−Am junction that has captivated our interest as it is considered the point where the 5f orbitals of the later actinides become more localized, nonbonding, and more lanthanide-like in behavior. Following this line of thought, curium should be more "lanthanide-like" than either plutonium or americium, and yet it behaves as if it were the transition between plutonium and americium. Yttrium, which does not possess any f-orbitals in its ground state, follows the expected trend of steric and ionic interactions in determination of the respective product and is isotypic with the later actinide product, Ln[$B_6O_9(OH)_3$].

Furthermore, it appears to us that while it is appropriate to consider steric and ionic factors and interactions as the main driving force in the bonding of the lanthanides, it is not so with the actinides. We think that it is the uniqueness of each actinide, especially with americium and curium that have historically been mislabeled as "lanthanide-like", that results in the structures observed. From CASSCF calculations, irrespective of structure and metal, the An 5f orbitals are fully localized and do not show bonding with coordinating groups. However, just below the valence An 5f orbitals, a Pu 6p orbital of **PuBOCl-1** and **PuBOCl-2** is observed with delocalized electron density on a basal O 2p orbital. For **AmBO**, **CmBO**, and **CmBOCl**, the equivalent An 6p orbital lies lower in energy below the An 5f orbitals, and instead a basal O 2p orbital shows delocalization to the An 6d orbital. It seems for the latter An^{3+} borate complexes, the An 6d participates in bonding even if very minimally. For **CeBOCl**, the electronic structure is analogous to the Pu complexes where the Ce 4f orbital is localized and noninteracting and the Ce 5p orbital shows no interaction with the coordinating ligands.

Insights differentiating the electronic structures of the An^{3+} borates were further identifiable from DFT-NBO and NPA calculations. The natural electronic configurations of the An 5f orbitals for **PuBOCl-1** and **PuBOCl-2** show an increase of 7.0 and 10.2% in electron occupation compared to that of **AmBO**, **CmBO**, and **CmBOCl** at 3.7, 2.7, and 2.4% respectively, indicating a larger transfer of electron density to Pu 5f. This is consistent with the expected localization and decreased involvement of the Am and Cm 5f orbitals given the consequent ionic contraction. The natural electronic configurations also indicate a unique involvement of the An 6d orbitals with the electron occupation of **PuBOCl-1** and **PuBOCl-2** being 0.2 and 0.1 e larger than the average of **AmBO**, **CmBO**, and **CmBOCl**, respectively.

Considering the total atomic populations allowed differentiation between the electronic structures of the An^{3+} borates indicating an increased occupancy of the An 5d orbitals irrespective of actinide metal and structure. For **PuBOCl-1** and **PuBOCl-2**, there was an increase of 10.9 and 9.6%, respectively, above the ideal $5d^{10}$ occupation, larger than the 8.6, 8.5, and 8.5% increase predicted for **AmBO**, **CmBO**, and **CmBOCl**, respectively, and indicative of a larger electron transfer and occupation of the Pu *5d* orbitals. Similarly, comparing the atomic populations of the An 5f orbitals highlights a distinction as there is a relative increase in electron population of the Pu 5f orbitals of 7.7 and 10.7% compared to 3.9, 2.8, and 2.6% for the Am and Cm 5f orbitals, as confirmed by the predicted natural electron configurations.

To fully grasp how similar the trivalent lanthanide and actinide borates are to each other, the other halogen analogues of both f-block series have been completed and the results are forthcoming. Also, we have begun work in exploring how trivalent neptunium and californium compare to the above results. It is our hope that our current (and future) results can shed some light on the true nature of the 4f and 5f orbitals, which may find applications in the areas of nuclear energy, storage, and separations.

■ ASSOCIATED CONTENT

Ⓢ Supporting Information

Information on the natural electronic configurations, atomic occupancies, Loewdin and natural population calculations as well as the atomic coordinates used for calculations, several molecular orbitals obtained at the CASSCF level, and the absorption spectra of the plutonium, americium, and curium species presented. This material is available free of charge via the Internet at http://pubs.acs.org.

■ AUTHOR INFORMATION

Corresponding Author

talbrec1@nd.edu

Notes

The authors declare no competing financial interest.

■ ACKNOWLEDGMENTS

We are grateful for support provided by the Chemical Sciences, Geosciences, and Biosciences Division, Office of Basic Energy Sciences, Office of Science, Heavy Elements Chemistry Program, U.S. Department of Energy, under Grant DE-FG02-09ER16026, which supports all of the synthetic, structural, and spectroscopic studies. Computational work was supported as part of the Materials Science of Actinides, an Energy Frontier Research Center funded by the U.S. Department of Energy, Office of Science, Office of Basic Energy Sciences under Award Number DE-SC0001089. Collaborative work with our German counterparts is supported via the Helmholtz Association, Grant Number: VH-NG-815.

■ REFERENCES

(1) Edelstein, N. M.; Fuger, J.; Katz, J. J.; Morss, L. R. *The Chemistry of the Actinide and Transactinide Elements*; Morss, L. R., Edelstein, N. M., Fuger, J., Eds.; Springer: The Netherlands, 2006.

(2) Shannon, R. D. *Acta Crystallogr., Sect. A* **1976**, *32*, 751−767.

(3) (a) Skanthakumar, S.; Antonio, M. R.; Wilson, R. E.; Soderholm, L. *Inorg. Chem.* **2007**, *46*, 3485−3491. (b) Apostolidis, C.; Schimmelpfennig, B.; Magnani, N.; Lindqvist-Reis, P.; Walter, O.; Sykora, R.; Morgenstern, A.; Colineau, E.; Caciuffo, R.; Klenze, R.; Haire, R. G.; Rebizant, J.; Bruchertseifer, F.; Fanghanel, T. *Angew. Chem., Int. Ed.* **2010**, *49*, 6343. (c) Matonic, J. H.; Scott, B. L.; Neu, M. P. *Inorg. Chem.* **2001**, *40*, 2638−2639.

(4) (a) Nash, K. L.; Lavallette, C.; Borkowski, M.; Paine, R. T.; Gan, X. *Inorg. Chem.* **2002**, *41*, 5849−5858. (b) Miguirditchian, M.; Guillaneux, D.; Guillaumont, D.; Moisy, P.; Madic, C.; Jensen, M. P.; Nash, K. L. *Inorg. Chem.* **2005**, *44*, 1404−1412.

(5) (a) Wang, S.; Alekseev, E. V.; Diwu, J.; Casey, W. H.; Phillips, B. L.; Depmeier, W.; Albrecht-Schmitt, T. E. *Angew. Chem., Int. Ed.* **2010**, *49*, 1057−1060. (b) Yu, P.; Wang, S.; Alekseev, E. V.; Depmeier, W.; Albrecht-Schmitt, T. E.; Phillips, B.; Casey, W. *Angew. Chem., Int. Ed.* **2010**, *49*, 5975−5977. (c) Wang, S.; Ping, Y.; Purse, B. A.; Orta, M. J.;

Diwu, J.; Casey, W. H.; Phillips, B. L.; Alekseev, E. A.; Depmeier, W.; Hobbs, D. T.; Albrecht-Schmitt, T. E. *Adv. Funct. Mater.* **2012**, In Press.

(6) (a) Wang, S.; Alekseev, E. V.; Ling, J.; Liu, G.; Depmeier, W.; Albrecht-Schmitt, T. E. *Chem. Mater.* **2010**, *22*, 2155−2163. (b) Wang, S.; Alekseev, E. V.; Stritzinger, J. T.; Depmeier, W.; Albrecht-Schmitt, T. E. *Inorg. Chem.* **2010**, *49*, 2948−2953. (c) Wang, S.; Alekseev, E. V.; Stritzinger, J. T.; Depmeier, W.; Albrecht-Schmitt, T. E. *Inorg. Chem.* **2010**, *49*, 6690−6696. (d) Wang, S.; Alekseev, E. V.; Stritzinger, J. T.; Liu, G.; Depmeier, W.; Albrecht-Schmitt, T. E. *Chem. Mater.* **2010**, *22*, 5983−5991. (e) Wang, S.; Alekseev, E. V.; Ling, J.; Skanthakumar, S.; Soderholm, L.; Depmeier, W.; Albrecht-Schmitt, T. E. *Angew. Chem., Int. Ed.* **2010**, *49*, 1263−1266. (f) Wang, S.; Villa, E. M.; Diwu, J.; Alekseev, E. V.; Depmeier, W.; Albrecht-Schmitt, T. E. *Inorg. Chem.* **2011**, *50*, 2527−2533. (g) Wang, S.; Alekseev, E. V.; Diwu, J.; Miller, H. M.; Oliver, A.; Liu, G.; Depmeier, W.; Albrecht-Schmitt, T. E. *Chem. Mater.* **2011**, *23*, 2931−2939.

(7) (a) Wang, S.; Alekseev, E. V.; Depmeier, W.; Albrecht-Schmitt, T. E. *Chem. Commun.* **2010**, *46*, 3955−3957. (b) Wang, S.; Alekseev, E. V.; Miller, H. M.; Depmeier, W.; Albrecht-Schmitt, T. E. *Inorg. Chem.* **2010**, *49*, 9755−9757.

(8) Wang, S.; Alekseev, E. V.; Depmeier, W.; Albrecht-Schmitt, T. E. *Inorg. Chem.* **2011**, *50*, 2079−2081.

(9) Polinski, M. J.; Wang, S.; Alekseev, E. V.; Depmeier, W.; Albrecht-Schmitt, T. E. *Angew. Chem., Int. Ed.* **2011**, *50*, 8891−8894.

(10) Polinski, M. J.; Wang, S.; Alekseev, E. V.; Depmeier, W.; Liu, G.; Haire, R. G.; Albrecht-Schmitt, T. E. *Angew. Chem., Int. Ed.* **2012**, *51*, 1869−1872.

(11) (a) Lu, P.; Wang, Y.; Lin, J.; You, L. *Chem. Commun.* **2001**, 1178−1179. (b) Li, L.; Lu, P.; Wang, Y.; Jin, X.; Li, G.; Wang, Y.; You, L.; Lin, J. *Chem. Mater.* **2002**, *14*, 4963−4968. (c) Li, L.; Jin, X.; Li, G.; Wang, Y.; Liao, F.; Yao, G.; Lin, J. *Chem. Mater.* **2003**, *15*, 2253−2260.

(12) Cong, R.; Yang, T.; Wang, Z.; Sun, J.; Liao, F.; Wang, Y.; Lin, J. *Inorg. Chem.* **2011**, *50*, 1767−1774.

(13) Sheldrick, G. M. *SADABS* 2001, Program for absorption correction using SMART CCD based on the method of Blessing: Blessing, R. H. *Acta Crystallogr.* **1995**, *A51*, 33.

(14) Hohenberg, P.; Kohn, W. *Phys. Rev.* **1964**, *136*, 864−871.

(15) Kohn, W.; Sham, L. J. *Phys. Rev.* **1965**, *140*, 1133−1138.

(16) Roos, B. O.; Taylor, P. R.; Siegbahn, P. E. M. *Chem. Phys.* **1980**, *48*, 157−173.

(17) Andersson, K.; Malmqvist, P. -Å.; Roos, B. O. *J. Chem. Phys.* **1992**, *96*, 1218−1228.

(18) Perdew, J. P.; Burke, K.; Ernzerhof, M. *Phys. Rev. Lett.* **1996**, *77*, 3865−3868.

(19) Schaefer, A.; Huber, C.; Ahlrichs, R. *J. Chem. Phys.* **1994**, *100*, 5829−5836. Eichkorn, K.; Weigend, F.; Treutler, O.; Ahlrichs, R. *Theor. Chem. Acc.* **1997**, *97*, 119−124.

(20) Cao, X. Y.; Dolg, M. *J. Chem. Phys.* **2001**, *115*, 7348−7356.

(21) Ahlrichs, R.; Bar, M.; Haser, M.; Horn, H.; Kolmel, C. *Chem. Phys. Lett.* **1989**, *162*, 165−169.

(22) Hess, B. A. *Phys. Rev. A* **1986**, *33*, 3742−3748.

(23) Roos, B. O.; Lindh, R.; Malmqvist, P. -Å.; Veryazov, V.; Widmark, P. O. *J. Phys. Chem. A* **2005**, *109*, 6575−6579.

(24) Aquilante, F.; Gagliardi, L.; Pedersen, T. B.; Lindh, R. *J. Chem. Phys.* **2009**, *130*, 154107−154116.

(25) Aquilante, F.; Pedersen, T. B.; Lindh, R.; Roos, B. O.; De Meras, A. S.; Koch, H. *J. Chem. Phys.* **2008**, *129*, 024113−024121.

(26) Aquilante, F.; Malmqvist, P. A.; Pedersen, T. B.; Ghosh, A.; Roos, B. O. *J. Chem. Theory Comput.* **2008**, *4*, 694−702.

(27) Aquilante, F.; Pedersen, T. B.; Lindh, R. *J. Chem. Phys.* **2007**, *126*, 194106−194117.

(28) Gagliardi, L.; Roos, B. O. *Chem. Soc. Rev.* **2007**, *36*, 893−903. Gagliardi, L. *J. Am. Chem. Soc.* **2003**, *125*, 7504−7505.

(29) La Macchia, G.; Brynda, M.; Gagliardi, L. *Angew. Chem., Int. Ed.* **2006**, *45*, 6210−6213.

(30) Gagliardi, L.; Heaven, M. C.; Krogh, J. W.; Roos, B. O. *J. Am. Chem. Soc.* **2005**, *127*, 86−91.

(31) Gagliardi, L.; La Manna, G.; Roos, B. O. *Faraday Discuss.* **2003**, *124*, 63−68.

(32) Grant, D. J.; Stewart, T. J.; Bau, R.; Miller, K. A.; Mason, S. A.; Gutman, M.; McIntyre, G. J.; Gagliardi, L.; Evans, W. J. *Inorg. Chem.* **2012**, *51*, 3613.

(33) Karlström, G.; Lindh, R.; Malmqvist, P. -Å.; Roos, B. O.; Ryde, U.; Veryazov, V.; Widmark, P. -O.; Cossi, M.; Schimmelpfennig, B.; Neogrady, P.; Seijo, L. *Comput. Mater. Sci.* **2003**, *287*, 222−239.

(34) Belokoneva, E. L.; Stefanovich, S.; Dimitrova, O. V.; Ivanova, A. G. *Zh. Neorg. Khim.* **2002**, *47*, 370−377.

(35) Ruiz-Martínez, A.; Alvarez, S. *Chem.—Eur. J.* **2009**, *15*, 1470−7480.

(36) Ruiz-Martínez, A.; Casanova, D.; Alvarez, S. *Chem.—Eur. J.* **2008**, *14*, 1291−1303.

(37) Borgoo, A.; Torrent-Sucarrat, M.; De Proft, F.; Geerlings, P. *J. Chem. Phys.* **2007**, *126*, 234104.

(38) Edelstein, N. M.; Lander, G. H.. *The Chemistry of the Actinide and Transactinide Elements*; Morss, L. R., Edelstein, N. M., Fuger, J., Eds.; Springer: The Netherlands, 2006; Vol. 3, Chapter 20.

(39) (a) Carnall, W. T.; Fields, P. R.; Pappalardo, R. G. *J. Chem. Phys.* **1970**, *53*, 2922. (b) Pappalardo, R. G.; Carnall, W. T.; Fields, P. R. *J. Chem. Phys.* **1969**, *51*, 1182. (c) Carnall, W. T.; Rajnak, K. *J. Chem. Phys.* **1975**, *63*, 3510.